Journal of Alloys and Compounds 525 (2012) 28–33

Contents lists available at SciVerse ScienceDirect

Journal of Alloys and Compounds

journal homepage: www.elsevier.com/locate/jallcom

Highly crystalline superparamagnetic iron oxide nanoparticles (SPION) in a silica matrix

Marin Tadić[a,*], Vladan Kusigerski[a], Dragana Marković[a], Matjaž Panjan[b], Irena Milošević[c,d], Vojislav Spasojević[a]

[a] Condensed Matter Physics Laboratory, Vinca Institute, University of Belgrade, POB 522, 11001 Belgrade, Serbia
[b] Jožef Stefan Institute, Jamova 39, 1000 Ljubljana, Slovenia
[c] Centre de Recherche sur la Matière Divisée, UMR 6619, CNRS-Université d'Orléans, 1b rue de la Férollerie, 45071 Orléans Cedex 2, France
[d] Laboratoire CSPBAT, UMR 7244 CNRS Université Paris 13, 93017 Bobigny Cedex, France

ARTICLE INFO

Article history:
Received 23 November 2011
Received in revised form 30 January 2012
Accepted 6 February 2012
Available online xxx

Keywords:
Superparamagnetism
Iron oxides
Nanostructures
Magnetic materials
Sol–gel synthesis
Magnetic measurements

ABSTRACT

We report on magnetic properties of iron oxide nanoparticles in a silica matrix synthesized by the sol–gel method. The sample is characterized by using X-ray powder diffractometer (XRPD), transmission electron microscopy (TEM), energy-dispersive X-ray spectroscopy (EDX) and superconducting quantum interference device (SQUID) magnetometer. TEM reveals iron oxide nanoparticles (maghemite/magnetite) of small sizes of about 4 nm, narrow size distribution and no particle agglomeration. The SQUID measurements show low blocking temperature $T_B = 6$ K and superparamagnetic behavior above 30 K. Obtained saturation magnetization $M_S = 61.1$ emu/g is very high, among the highest values for iron oxides of particle size below 5 nm. The field-cooled hysteresis measurements do not show displacement of the hysteresis loop thus indicating an absence of exchange bias, whereas AC susceptibility reveals non-interacting nanoparticles. The values of K_{eff} and K_S (effective and surface anisotropy constants) obtained in this work are smaller than those reported in the literature for systems where shell's disorder spin structure (surface effects) is observed. These results point to highly crystalline iron oxide nanoparticles with a low amount of internal defects and small surface disorder shell thickness which is uncommon for nanoparticles of this size. Superparamagnetic iron oxide nanoparticles (SPION) with such properties are convenient for the biomedical applications in targeted diagnostics and drug delivery.

1. Introduction

One of the most interesting and active research topics in materials science during the last few years is the investigation of nanosized iron oxides [1–38]. Several types of iron oxides exist in nature and can be prepared in the laboratory, but nowadays maghemite and magnetite are widely used for biomedical applications. The useful properties of maghemite and magnetite for biomedical applications include sufficiently high magnetic moments, chemical stability, low toxicity, easy and economical synthesis of these materials. The generic names "iron oxide" and/or "superparamagnetic iron oxide nanoparticles (SPION)" are common in the literature; their meaning being understood as either maghemite and/or magnetite, without pointing out any particular one [39–44]. Interest in their preparation and investigation is currently driven by a wide range of potential applications, such as information storage, sensors, catalyst, pigments, water decontamination, adsorbents, enzyme supports, targeted drug delivery, tissue engineering, local hyperthermia, ferrofluids and contrast agents in nuclear magnetic resonance imaging [1,2,32–55].

Complex magnetic properties of nanosized iron oxides have been widely discussed and a wide range of magnetic properties has been obtained [1,8–36,56–62]. Dutta et al. reported nearly defect-free maghemite nanocrystals of a size of about 7 nm, high saturation magnetization $M_S = 80$ emu/g close to bulk value, whereas at the same time, very low coercivity $H_C = 20$ Oe was obtained [63]. On the other hand, Martinez et al. reported high value of coercivity $H_C = 3000$ Oe and a very low saturation magnetization $M_S = 5$ emu/g in nanosized maghemite [64]. A recent paper by Han et al. reported on magnetite nanowires with non-zero coercivity $H_C = 310$ Oe at room temperature [65] whereas Ennas et al. obtained Fe_2O_3/SiO_2 nanocomposite with low blocking temperature $T_B = 6$ K [66]. Cannas et al. reported two samples of Fe_2O_3 nanoparticles dispersed in an amorphous SiO_2 matrix with average diameters of 3 nm and 6 nm, blocking temperatures of 10 K and 22 K, saturation magnetizations of 43.7 emu/g and

* Corresponding author. Tel.: +381 11 8065828; fax: +381 11 8065829.
E-mail address: marint@vinca.rs (M. Tadić).

0925-8388/$ – see front matter © 2012 Elsevier B.V. All rights reserved.
doi:10.1016/j.jallcom.2012.02.056

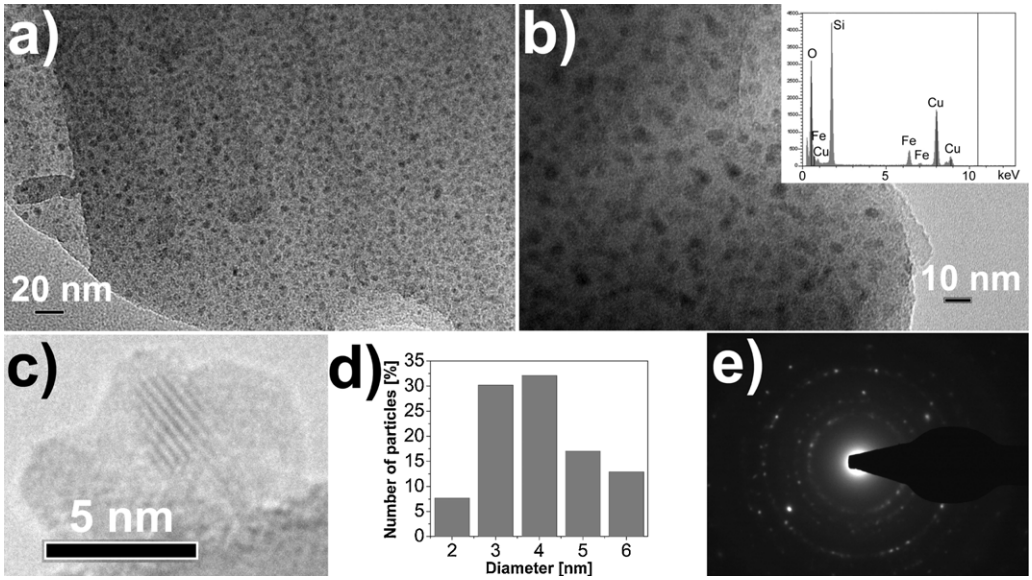

Fig. 1. (a) and (b) TEM images of the sample whereas inset shows EDX spectrum; (c) HRTEM image of an iron oxide nanoparticle; (d) size distribution of iron oxide nanoparticles; (e) SAED pattern of the nanocrystals.

37.8 emu/g, and coercivities of 810 Oe and 1180 Oe, respectively [67]. Nadeem et al. prepared ultrafine maghemite nanoparticles with size of about 4 nm, high coercivity of 3008 Oe and low saturation magnetization [68]. These magnetic properties arise both from the atoms which reside on the surface of the nanoparticles, and from the finite number of atoms in the nanoparticle crystalline core. It has been shown that particle size, morphology, defects, core–shell and dipolar interactions have a large influence on the magnetic properties of the samples [1,8–38,56,62,63,65,67–74]. Moreover, the finite size and surface effects are usually masked by the presence of particle size distribution and by a magnetic interaction between the particles, and it is very difficult to distinguish the real contribution of finite size and surface effects on the magnetic properties. Consequently, preparation of the magnetic nanoparticles requires several tasks, such as control of the size and size distribution of the particles, control of the morphology and crystallinity, and prevention of the agglomeration. Different preparation methods have been developed in order to obtain desirable samples and physical properties: hydrothermal, sol–gel, solvothermal, mechanochemical, polyol process, co-precipitation, template, thermal decomposition, spray pyrolysis, chemical vapour deposition, carbothermal reduction, electro-precipitation, microwave plasma synthesis, γ-irradiated water-in-oil microemulsion, melt quench technique, microemulsion and reverse microemulsion technique [1,6–26,48,59,62,68,70,73–80]. Among them the sol–gel method has been shown to be very useful for preparation of iron oxide nanoparticles dispersed in an amorphous silica matrix. Silica is convenient because of its nontoxic nature, high biocompatibility, prevention of agglomeration, temperature resistance, chemical inertness and adjustable pore diameter [1,2,8,10,21,32,36,37,49,50,52–54,57,61,67,81–84].

In this paper, we report the synthesis and magnetic properties of highly crystalline iron oxide nanoparticles of about 4 nm size with a narrow particle size distribution. Magnetic measurements are in good agreement with TEM observations and show very interesting magnetic properties such as high saturation magnetization M_S = 61.1 emu/g, low blocking temperature T_B = 6 K, superparamagnetic behavior above 30 K, coercivity H_C = 390 Oe at 2 K, absence of exchange bias and AC susceptibility behavior well described by the Neel–Arrhenius model for single domain non-interacting nanoparticles.

2. Experimental

The sample was prepared using the sol–gel method. The starting point for the synthesis of a targeted system was a solution prepared by mixing tetraethylorthosilicate (TEOS), water and ethanol. An aqueous solution of iron nitrate ($Fe(NO_3)_3 \cdot 9H_2O$, Aldrich 98%) was added to the initial solution in such a proportion as to provide the 10 wt.% of iron oxide (Fe_2O_3) in the final dried powder. The mole ratios of ethanol to TEOS and water to TEOS were 4:1 and 12:1, respectively. After an hour of stirring the pH of the mixture settled at about 3. The clear sol was poured into a glass beaker and allowed to gel in the air. The gel was dried for about ten days at 80 °C temperature. The sample was finally heated in air at 900 °C for 5 hour. The obtained sample is brown in color.

The size and morphology of the nanoparticles was investigated by transmission electron microscope (TEM), using a Phillips CM20 instrument. Element components were determined using energy-dispersive X-ray spectroscopy (EDX) provided in the TEM.

Magnetic measurements were performed on a commercial Quantum Design MPMS XL-5 SQUID-based magnetometer in a wide range of temperatures (2–300 K) and applied DC fields (up to 5 T). The same instrument was used for AC magnetization measurements carried out in the 1 Hz ≤ ν ≤ 1000 Hz frequency range and in a temperature region encompassing blocking temperatures.

3. Results and discussion

The transmission electron microscopy (TEM) images, size distribution, EDX spectrum and selected area electron diffraction (SAED) pattern are shown in Fig. 1. The TEM images show formation of nanoparticles and uniform dispersion of the nanoparticles in the amorphous silica matrix (Fig. 1(a) and (b)). No agglomeration of particles has been observed suggesting isolated nanoparticles and a non-interacting system. Fig. 1(c) shows the high-resolution TEM picture of a nanoparticle and reveals lattice fringe pattern demonstrating a well-crystallized structure. Fig. 1(d) presents a size distribution of nanoparticles, where symmetrical size dispersion with an average size of about 4 nm can be seen. Moreover, a narrow size distribution is showed. The particle size distribution of sample is fitted by a log-normal distribution function. The standard deviation of σ = 0.11 is obtained from such a fit. The selected area electron diffraction (SAED) pattern shown in Fig. 1(e) consists of diffraction spots/rings that were indexed in correspondence to the maghemite/magnetite spinel structure ((4 4 0), (5 1 1), (4 2 2), (4 0 0), (3 1 1) and (2 2 0) planes are observed which appropriate to spots/rings of smaller to larger diameters, respectively). Also, the periodic fringe spacing of ∼3 Å corresponds to the (2 2 0) planes

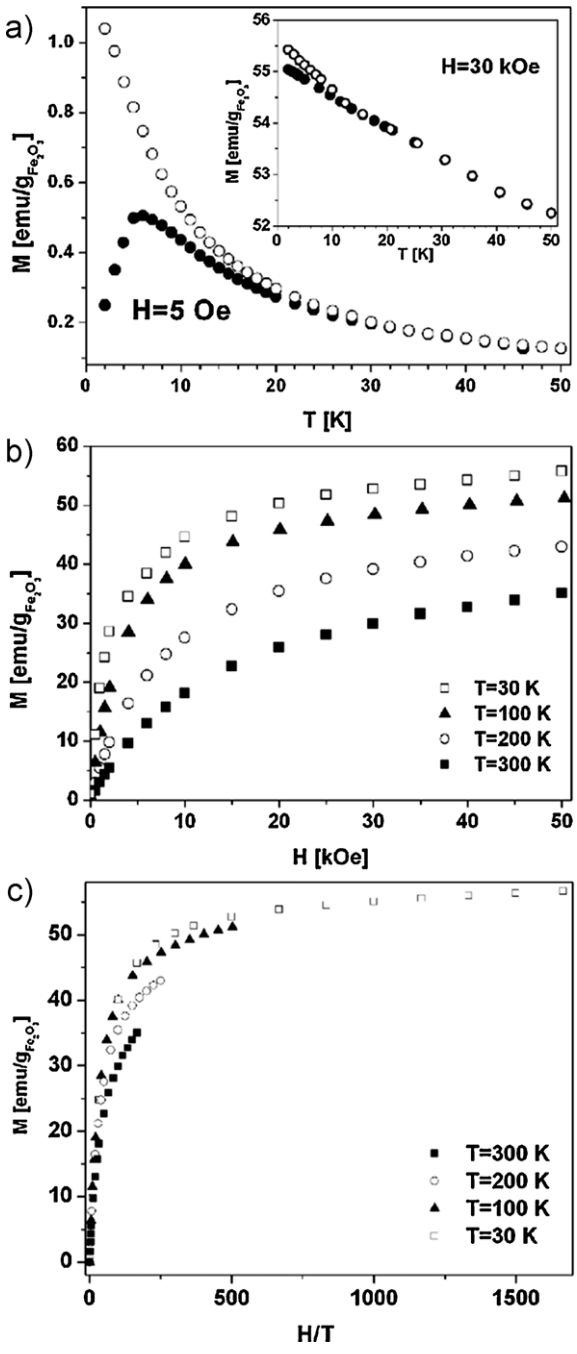

Fig. 2. Temperature dependence of the zero-field-cooled (ZFC, solid symbols) and field-cooled (FC, open symbols) magnetization measured in a field of 5 Oe and 30 kOe (inset); (b) magnetization of the sample at several temperatures expressed as a function of the applied field *H*.

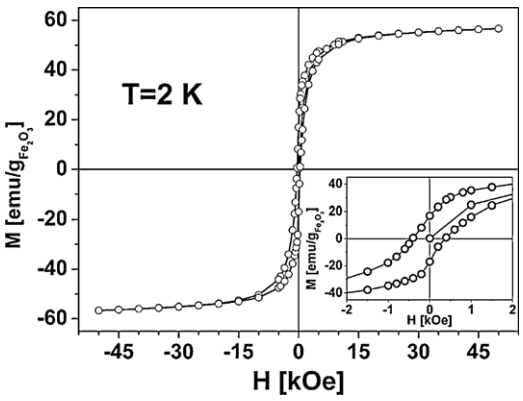

Fig. 3. Magnetization vs. field dependence recorded at 2 K. The inset shows low field magnetization behavior.

of maghemite/magnetite structure were revealed (Fig. 1(c)). Inset of Fig. 1(b) shows the EDX spectrum of the Fe_2O_3/SiO_2 nanocomposite, where Fe, Si and O are the main components. Their atomic ratios are in a good agreement with those expected from synthesis conditions. The Cu peaks in the EDX spectrum originate from the copper web which is used for the preparation of the sample for EDX observation. No other impurities have been identified. The X-ray diffraction measurement shows only a very broad reflection due to the amorphous silica matrix (90 wt.%) covering the nanocrystalline iron oxide reflections which are expected to be broad because of the small particle size (figure is not shown). Fig. 2(a) shows the temperature dependence of the zero-field-cooled (ZFC) and field-cooled (FC) magnetization from 2 to 80 K under low DC field of 5 Oe. The ZFC curve exhibits a single narrow maximum with the peak value at very low temperature $T_B = 6$ K (blocking temperature). Below T_B, the FC and ZFC magnetization curves split significantly, the ZFC magnetization decreases sharply whereas the FC magnetization increases continuously down to 2 K, which is usually considered a characteristic of non-interacting nanoparticles or weak interacting nanoparticles [8,61]. Above 6 K, the FC and ZFC magnetization curves exhibit the same trend and at the irreversibility temperature $T_{irr} = 28$ K the curves coincide, pointing out that all nanoparticles are in the superparamagnetic state. In the case of non-interacting nanoparticles the temperature at which the ZFC and the FC curves separate ($T_{irr} = 28$ K) corresponds to the blocking temperature of the largest particles whereas the maximum of the ZFC curve ($T_B = 6$ K) can be related to the blocking of the average sized particles. The low blocking temperature, narrow peak in the ZFC magnetization and small difference $T_{irr} - T_B = 22$ K (Fig. 2(a)) point to ultra small particles and narrow size distribution which is in agreement with TEM observations. In addition, the ZFC and FC curves do not coincide in a field of 30 kOe (Fig. 2(a), inset). Fig. 2(b) shows a field dependence of isothermal magnetization at 30, 100, 200 and 300 K (above $T_{irr} = 28$ K) showing no hysteretic properties ($H_C = 0$ Oe, $M_r = 0$ emu/g). This confirms superparamagnetic behavior which is expected from the $M(T)$ measurements. The same magnetization data are presented in Fig. 2(c) as a function of H/T. If the sample were truly superparamagnetic, then the magnetization curves measured at different temperatures could be superimposed when magnetization is plotted as a function of H/T. This feature is indeed achieved as can be seen in Fig. 2(c), thus confirming the superparamagnetic behavior of our sample for temperatures above 30 K.

The field dependence of isothermal magnetization was recorded at 2 K (ZFC hysteresis measurements), i.e. below T_B, in the field range of ±5 T. In Fig. 3, it can be seen that the magnetization is almost saturated for high field values as observed for well-crystallized ferrimagnetic iron oxide nanomaterials [9,54,58,63]. The obtained hysteresis loop is symmetric around the origin (Fig. 3, inset), with coercivity, remanence and saturation magnetization $H_C = 390$ Oe, $M_r = 17.2$ emu/g, and $M_S = 61.1$ emu/g, respectively. The value of M_S was determined by extrapolating $1/H$ to zero-field in the M vs. $1/H$ plot based on the high field data. The obtained value of M_S is among the highest values obtained for iron oxide materials of particle sizes below 5 nm. The obtained high value of the M_S points to highly crystalline iron oxide nanoparticles with low amount of internal defects and small surface magnetic disorder (i.e. low shell thickness) which is uncommon for nanoparticles in this size range (<5 nm) [56]. Surface effects and internal defects have been reported as being responsible for the reduction of the

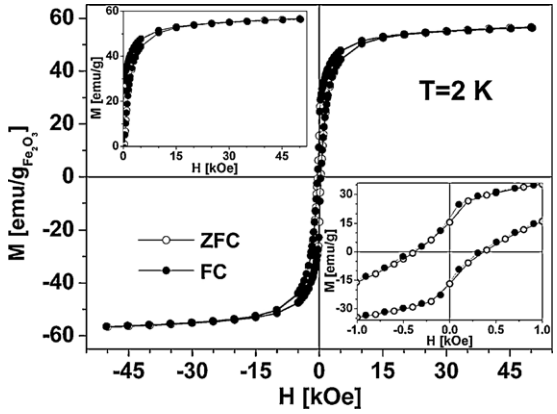

Fig. 4. ZFC and FC hysteresis loops at 2 K, ZFC (ZFC, solid symbols) and FC (FC, open symbols after cooling in 30 kOe). The inset shows the low field magnetization response.

saturation magnetization of the ferrimagnetic iron oxide nanoparticles [1,12,16,18,22,25,56,64,67,68,84]. To gain further insight into the origin of the high magnetization of the iron oxide nanoparticles, a field-cooled (FC) hysteresis loop has been recorded (Fig. 4). The FC hysteresis loop was measured after cooling the sample in an applied field of 50 kOe from 200 K temperature down to 2 K. The FC magnetization curve does not exhibit the typical features of an exchange bias (Fig. 4), i.e. a shift of the hysteresis loop and/or enhanced coercivity [15,64,69,71,84]. These features occur in nanoparticle systems due to the exchange coupling between the different core and surface magnetic structures [15,64,69,71,84]. We assume that because of the high crystallinity of the nanoparticles and very thin disorder surface layers of the nanoparticles, the exchange bias effect is not observed in the sample. Magnetic hysteresis measurements at different temperatures were performed in order to get more information about magnetic properties of the nanoparticles. Fig. 5(a) shows the variation of the coercivity with temperature for the sample (2 K, 2.5 K, 3 K, 4 K, 5 K and 6 K). It is apparent from this figure that the coercivity is strongly dependent on temperature, as expected for nanoparticle systems. At higher temperature, the particles have higher thermal energy, and hence, they require smaller field to reverse the magnetization. The coercivity for a system of non-interacting particles is expected to follow relation:

$$H_C = H_{C_0}\left[1 - \left(\frac{T}{T_B}\right)^{1/2}\right], \quad (1)$$

where H_{C_0} is the coercivity at 0 K. The fit of the experimental data to Eq. (1) is given in Fig. 5(b) (solid line) where we plot the coercivity with respect to the $T^{1/2}$ [12,21,85–88]. The extrapolation of $H_C(T)$ to zero field and zero temperature yield for our sample the value of T_B = 6.4 K and H_{C_0} = 770 Oe. We notice that the blocking temperature determined by the hysteresis measurements agrees well with the ZFC/FC results. The fit in Fig. 5(b) is not fully seen in accordance with the measured data, which is also observed in similar systems and this is not well understood and demands further investigation [85].

In order to investigate the dynamic behavior of the nanoparticles, we performed AC susceptibility measurements at five different frequencies (1, 10, 100, 500 and 1000 Hz) in the temperature range 2–30 K that encompasses the blocking temperature. Fig. 6(a) and (b) shows the plots of χ' and χ'' against temperature for the nanocomposite. It can be noted that the χ' peak is at higher temperatures than the peak for χ'' at the same frequencies, the peak positions shift to higher temperatures with increasing frequency ν_{ac} for both χ' and χ'' and the value of χ' decreases whereas

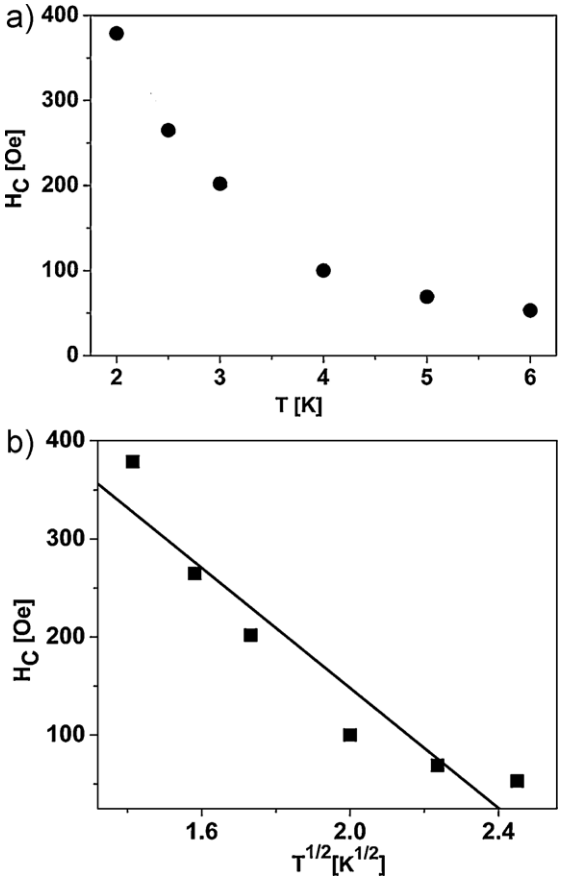

Fig. 5. Temperature dependence of coercivity for the sample (2 K, 2.5 K, 3 K, 4 K, 5 K and 6 K); (b) shows H_C plot with respect to $T^{1/2}$.

the χ'' increases with increasing frequency. These properties are also observed in other nanoparticle systems [68,77,84,89]. The presence of inter-particle interactions can be revealed from the frequency dependence of T_B by using the empirical parameter $C_1 = \Delta T_B/(T_B \Delta \log \nu)$, where T_B denotes the average value of blocking temperature in the range of experimental frequencies, whereas ΔT_B denotes the difference between maximum and minimum value of T_B (Fig. 6(a)). In this way C_1 = 0.1055 was obtained. That value lies in the range ~0.1 to 0.13 which is expected for non-interacting nanoparticles [94]. The interaction between particles can be classified as the long-range magnetostatic dipole–dipole interaction and the exchange coupling interaction of neighboring particles [85,90–94]. The non-interacting nanoparticles denote isolated nanoparticles without dipolar and exchange inter-particle interactions [85,90–94]. According to the Neel theory of superparamagnetism [95], the magnetic moments of non-interacting single domain identical particles with uniaxial anisotropy fluctuate between two directions of easy axes with a relaxation time τ that obeys the Arrhenius law:

$$\tau = \tau_0 \exp\left(\frac{E_a}{k_B T_B}\right), \quad (2)$$

where E_a is the anisotropy energy, τ is the measurement time, and τ_0 is the attempt frequency. The temperature corresponding to the maximum of the AC susceptibility (Fig. 6(a)) can be identified with the blocking temperature, i.e., the temperature at which the relaxation time is equal to the time scale of the experiment τ which, in an AC susceptibility experiment is given by the reverse of the measuring frequency, $\tau = 1/\nu_{ac}$. Below T_B, the relaxation times of the particles are longer than the experimental time τ and particles are in the blocking state whereas above T_B, the τ is longer than

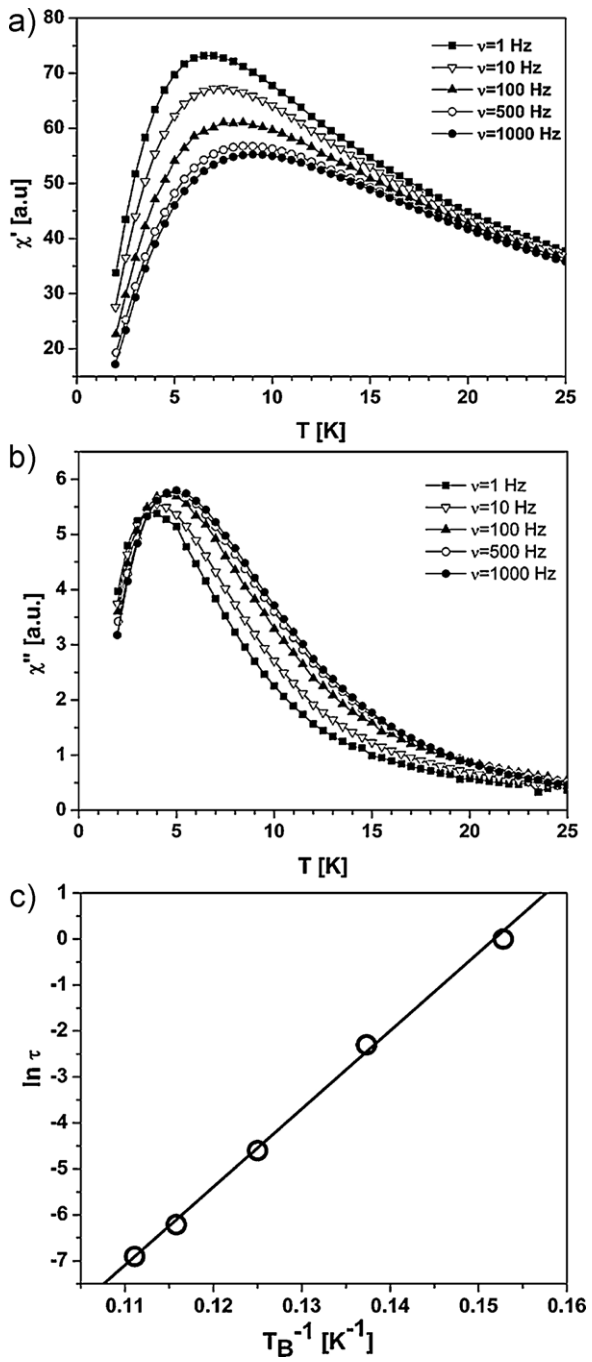

Fig. 6. Temperature dependence of the real χ' (a) and imaginary χ'' (b) part of AC susceptibility at different frequencies; (c) change of blocking temperatures T_B with AC field frequency ν fitted to the Arrhenius function.

the relaxation times of the particles and the particles are in the superparamagnetic state. The values of T_B in Fig. 6(c) are determined as maximums of AC susceptibility in Fig. 6(a). In the case of non-interacting particles the dependence of $\ln \nu$ vs. $T_B{}^{-1}$ should be linear, whereas the attempt frequency τ_0 is usually within the 10^{-9} to 10^{-12} range. The fit of the experimental data to Eq. (2) is given in Fig. 6(c) (solid line), where the best fit values obtained are $\tau_0 = 2.43\,10^{-12}$ s and $E_a/k_B = 169.8$ K. The value of $\tau_0 \sim 10^{-12}$ s determined from the fit of our experimental data to the Arrhenius law (Fig. 6(c)) is in the above quoted range. This confirms the non-interacting nanoparticles in our nanoparticle system, which is in agreement with TEM observations and $M(T)$ measurements. The magnetic anisotropy parameter E_a/k_B can be used to estimate the effective anisotropy constant K_{eff}, using the relation $K_{eff}V = E_a$, where V denotes the volume of a particle. For a particle with diameter $d = 4$ nm, this relation gives $K_{eff} = 8.741\,10^4$ erg/cm^3. The temperature of the maximum of the ZFC magnetization ($T_B = 6$ K), which is related to the mean blocking temperature T_B of the particle assembly, can also be used to give an estimate of the effective anisotropy constant K_{eff} through the relation $K_{eff} = 25k_BT_B/V$, valid under the assumption of non-interacting nanoparticles. For $d = 4$ nm, $K_{eff} = 7.722\,10^4$ erg/cm^3. We notice a good agreement with values obtained by AC and DC SQUID measurements and both values are close to bulk and nearly defect-free iron oxide nanoparticles [63]. Moreover, the surface anisotropy K_S can be deduced as $K_S = K_{eff}D/6$, where D is the particle diameter ($D = 4$ nm) [86]. We obtained a value of $K_S \approx 5.5\,10^{-3}$ erg/cm^2. The values obtained in this work (K_{eff} and K_S) are smaller than those reported in the literature for systems where shell's disorder spin structure is observed [12,68,84,96]. This also points to a highly crystalline iron oxide nanoparticles and agrees with the $M(H)$ and TEM results.

4. Conclusions

The sol–gel method was utilized for the synthesis of iron oxide nanoparticles in an amorphous silica matrix. TEM images show well-crystallized iron oxide nanoparticles with an average size of about 4 nm and narrow size distribution without particle agglomeration. These observations emphasize the sol–gel method as suitable for synthesis of the ultra small uniformly sized nanoparticle systems. The magnetic properties are in a good agreement with TEM observations and exhibit a low blocking temperature $T_B = 6$ K, the superparamagnetic behavior above 30 K, high saturation magnetization $M_S = 61.1$ emu/g, low coercivity $H_C = 390$ Oe, absence of exchange bias, and non-interacting nanoparticles. The values of K_{eff} and K_S (effective and surface anisotropy constants) obtained in this work are smaller than those reported in the literature for systems where shell's disorder spin structure is observed. These results point to highly crystalline iron oxide nanoparticles with low amount of internal defects and small magnetically disorder shell thickness which is uncommon for nanoparticles in this size range. The magnetic field directed SPION provide potential applications in targeted diagnostics and therapy. The superparamagnetic properties, high magnetization for easy control of their movement in blood by a magnetic field, and narrow size distribution i.e. uniform byophysicochemical properties show that investigated SPION are convenient for the biomedical applications in targeted diagnostics and drug delivery [1,2,45].

Acknowledgement

M.T. acknowledges Professor Veljko Dmitrasinović (Institute for Physics, Belgrade) for his comments. We thank Fabienne Warmont (CRMD, Orléans, France) for TEM observations. The Serbian Ministry of Science supported this work financially (Grant no. III 45015).

References

[1] A.S. Teja, P.Y. Koh, Prog. Cryst. Growth Charact. Mater. 55 (2009) 22–45.
[2] A.K. Gupta, M. Gupta, Biomaterials 26 (2005) 3995–4021.
[3] J.L. Perez-Rodriguez, C. Maqueda, N. Murafa, J. Šubrt, V. Balek, P. Pulišová, A. Lančok, Appl. Clay Sci. 51 (2011) 274–282.
[4] Z. Orolínová, A. Mockovčiaková, V. Zeleňák, M. Myndyk, J. Alloys Compd. 511 (2012) 63–69.
[5] G. Tong, W. Wu, J. Guan, H. Qian, J. Yuan, W. Li, J. Alloys Compd. 509 (2011) 4320–4326.
[6] C.Y. Yin, M. Minakshi, D.E. Ralph, Z.T. Jiang, Z. Xie, H. Guo, J. Alloys Compd. 509 (2011) 9821–9825.
[7] S. Gurmen, B. Ebin, J. Alloys Compd. 492 (2010) 585–589.
[8] M. Tadić, D. Marković, V. Spasojević, V. Kusigerski, M. Remškar, J. Pirnat, Z. Jagličić, J. Alloys Compd. 441 (2007) 291–296.

[9] R.A. Bini, R.F.C. Marques, F.J. Santos, J.A. Chaker, M. Jafelicci Jr., J. Magn. Magn. Mater. 324 (2012) 534–539.
[10] I. Ursachi, A. Vasile, A. Ianculescu, E. Vasile, A. Stancu, Mater. Chem. Phys. 130 (2011) 1251–1259.
[11] V. de Castro, G. Benito, S. Hurst, C.J. Serna, M.P. Morales, S. Veintemillas-Verdaguer, Thin Solid Films 519 (2011) 7677–7682.
[12] T. Tsuzuki, F. Schäffel, M. Muroi, P.G. McCormick, J. Alloys Compd. 509 (2011) 5420–5425.
[13] H. Wang, W.C. Geng, Res. Chem. Intermed. 37 (2011) 523–529.
[14] Y. Zhu, F.Y. Jiang, K. Chen, F. Kang, Z.K. Tang, J. Alloys Compd. 509 (2011) 8549–8553.
[15] S.K. Sharma, J.M. Vargas, K.R. Pirota, Shalendra Kumar, C.G. Lee, M. Knobel, J. Alloys Compd. 509 (2011) 6414–6417.
[16] S. Asuha, B. Suyala, X. Siqintana, S. Zhao, J. Alloys Compd. 509 (2011) 2870–2873.
[17] Y.J. Zhang, Y.W. Lin, C.C. Chang, T.M. Wu, Synth. Met. 160 (2010) 1086–1091.
[18] I.V. Vasylenko, S.V. Kolotilov, I.E. Kotenko, K.S. Gavrilenko, F. Tuna, G.A. Timco, R.E.P. Winpenny, V.V. Pavlishchuk, J. Magn. Magn. Mater. 324 (2012) 595–601.
[19] F. Zhao, B. Zhang, L. Feng, Mater. Lett. 68 (2012) 112–114.
[20] Md. Nazrul Islam, L. Van Phong, Jong-Ryul Jeong, CheolGi Kim, Thin Solid Films 519 (2011) 8277–8279.
[21] I. Šimkienė, M. Treideris, G. Niaura, R. Szymczak, P. Aleshkevych, A. Rėza, I. Kašalynas, V. Bukauskas, G.J. Babonas, Mater. Chem. Phys. 130 (2011) 1026–1032.
[22] J. Feng, J. Mao, X. Wen, M. Tu, J. Alloys Compd. 509 (2011) 9093–9097.
[23] E. Karaoğlu, A. Baykal, H. Erdemi, L. Alpsoy, H. Sozeri, J. Alloys Compd. 509 (2011) 9218–9225.
[24] S. Bahceci, B. Unal, A. Baykal, H. Sözeri, E. Karaoğlu, B. Esat, J. Alloys Compd. 509 (2011) 8825–8831.
[25] P. Hu, S. Zhang, H. Wang, D. Pan, J. Tian, Z. Tang, A.A. Volinsky, J. Alloys Compd. 509 (2011) 2316–2319.
[26] M.M. Can, T. Firat, S. Özcan, Physica B 406 (2011) 2483–2487.
[27] B. Faure, G. Salazar-Alvarez, L. Bergström, Langmuir 27 (2011) 8659–8664.
[28] R. Amutha, M. Muruganandham, M. Sathish, S. Akilandeswari, Rominder P.S. Suri, E. Repo, M. Sillanpää, J. Phys. Chem. C 115 (2011) 6367–6374.
[29] K. Mandel, F. Hutter, C. Gellermann, G. Sextl, Colloids Surf. A: Physicochem. Eng. Aspects 390 (2011) 173–178.
[30] M.A. Morales, A.J.S. Mascarenhas, A.M.S. Gomes, C.A.P. Leite, H.M.C. Andrade, C.M.C. de Castilho, F. Galembeck, J. Colloid Interface Sci. 321 (2010) 269–277.
[31] D. Amara, S. Margel, J. Mater. Chem. 21 (2011) 15764.
[32] S. Gandhi, S. Venkatesh, U. Sharma, N.R. Jagannathan, S. Sethuraman, U.M. Krishnan, J. Mater. Chem. 21 (2011) 15698.
[33] H. Yuan, Y. Wang, S.M. Zhou, S. Lou, Chem. Eng. J. 175 (2011) 555–560.
[34] G. Ghosh, A. Vilchez, J. Esquena, C. Solans, C. Rodríguez-Abreu, Mater. Chem. Phys. 130 (2011) 786–793.
[35] B. Bajaj, B.D. Malhotra, S. Choi, Thin Solid Films 519 (2010) 1219–1223.
[36] I. Ursachi, A. Vasile, H. Chiriac, P. Postolache, A. Stancu, Mater. Res. Bull. 46 (2011) 2468–2473.
[37] G.A. Bukhtiyarova, M.A. Shuvaeva, O.A. Bayukov, S.S. Yakushkin, O.N. Martyanov, J. Nanopart. Res. 13 (2011) 5527–5534.
[38] Q. Wang, X. Yang, L. Yu, H. Yang, J. Alloys Compd. 509 (2011) 9098–9104.
[39] M.I. Khan, A. Mohammad, G. Patil, S.A.H. Naqvi, L.K.S. Chauhan, I. Ahmad, Biomaterials 33 (2012) 1477–1488.
[40] T.H. Chung, J.K. Hsiao, S.C. Hsu, M. Yao, Y.C. Chen, S.W. Wang, M.Y.P. Kuo, C.S. Yang, D.M. Huang, ACS Nano 5 (2011) 9807–9816.
[41] S.S. Yu, R.L. Scherer, R.A. Ortega, C.S. Bell, C.P. O'Neil, J.A. Hubbell, T.D. Giorgio, J. Nanobiotechnol. 9 (2011) 7.
[42] W. He, F. Yang, Y. Wu, S. Wen, P. Chen, Y. Zhang, N. Gu, Mater. Lett. 68 (2012) 64–67.
[43] S. Ghoshal, A.A. Ansar, S.O. Raja, A. Jana, N.R. Bandyopadhyay, A.K. Dasgupta, M. Ray, Nanoscale. Res. Lett. 6 (2011) 540.
[44] V. Salgueirino-Maceira, M.A. Correa-Duarte, M. Spasova, L.M. Liz-Marzan, M. Farle, Adv. Funct. Mater. 16 (2006) 509–514.
[45] M. Mahmoudi, S. Sant, B. Wang, S. Laurent, T. Sen, Adv. Drug Deliv. Rev. 63 (2011) 24–46.
[46] K. Herve, L. Douziech-Eyrolles, E. Munnier, S. Cohen-Jonathan, M. Souce, H. Marchais, P. Limelette, F. Warmont, M.L. Saboungi, P. Dubois, I. Chourpa, Nanotechnology 19 (2008) 465608.
[47] Z.T. Tsai, J.F. Wang, H.Y. Kuo, C.R. Shen, J.J. Wang, T.C. Yen, J. Magn. Magn. Mater. 322 (2010) 208–213.
[48] H. Basti, L.B. Tahar, L.S. Smiri, F. Herbst, M.-J. Vaulay, F. Chau, S. Ammar, S. Benderbous, J. Colloid Interface Sci. 341 (2010) 248–254.
[49] U. Maver, M. Bele, D. Makovec, S. Čampelj, J. Jamnik, M. Gaberšček, J. Magn. Magn. Mater. 19 (2009) 3187–3192.
[50] V. Zelenak, A. Zelenakova, J. Kovac, U. Vainio, N. Murafa, J. Phys. Chem. C 113 (2009) 13045–13050.
[51] C.M. Cheng, G. Kou, X.L. Wang, S.H. Wang, H.C. Gu, Y.J. Guo, J. Magn. Magn. Mater. 321 (2009) 2663–2669.
[52] D. Chen, M. Jiang, N. Li, H. Gu, Q. Xu, J. Ge, X. Xia, J. Lu, J. Mater. Chem. 20 (2010) 6422–6429.
[53] C. Vogt, M.S. Toprak, M. Muhammed, S. Laurent, J.L. Bridot, R.N. Muller, J. Nanopart. Res. 12 (2010) 1137–1147.
[54] C. Wang, Y. Ao, P. Wang, J. Qian, J. Hou, S. Zhang, J. Alloys Compd. 493 (2010) 410–414.
[55] A. Mitra, C.V. Vazquez, M.A.L. Quintela, B.K. Paul, A. Bhaumik, Microporous Mesoporous Mater. 131 (2010) 373–377.
[56] M.P. Morales, S. Veintemillas-Verdaguer, M.I. Montero, C.J. Serna, A. Roig, L. Casas, B. Martinez, F. Sandiumenge, Chem. Mater. 11 (1999) 3058–3064.
[57] D. Ortega, R. Garcia, R. Marin, C. Barrera-Solano, E. Blanco, M. Dominguez, M. Ramirez-del-Solar, Nanotechnology 19 (2008) 475706.
[58] J. Drbohlavova, R. Hrdy, V. Adam, R. Kizek, O. Schneeweiss, J. Hubalek, Sensors 9 (2009) 2352–2362.
[59] H. Zhu, D. Yang, L. Zhu, H. Yang, D. Jin, K. Yao, J. Mater. Sci. 42 (2007) 9205–9209.
[60] W. Wu, X. Xiao, S. Zhang, H. Li, X. Zhou, C. Jiang, Nanoscale. Res. Lett. 4 (2009) 926–931.
[61] D. Makovec, S. Čampelj, M. Bele, U. Maver, M. Zorko, M. Drofenik, J. Jamnik, M. Gaberšček, Colloids Surf. A: Physicochem. Eng. Aspects 334 (2009) 74–79.
[62] V. Kusigerski, M. Tadić, V. Spasojević, B. Antić, D. Marković, S. Bošković, B. Matović, Scr. Mater. 56 (2007) 883–886.
[63] P. Dutta, A. Manivannan, M.S. Seehra, N. Shah, G.P. Huffman, Phys. Rev. B 70 (2004) 174428.
[64] B. Martinez, X. Obradors, L. Balcells, A. Rouanet, C. Monty, Phys. Rev. Lett. 80 (1998) 181–184.
[65] Q. Han, Z. Liu, Y. Xu, H. Zhang, J. Cryst. Growth 307 (2007) 483–489.
[66] G. Ennas, A. Musinu, G. Piccaluga, D. Zedda, D. Gatteschi, C. Sangregorio, J.L. Stanger, G. Concas, G. Spano, Chem. Mater. 10 (1998) 495–502.
[67] C. Cannas, G. Concas, D. Gatteschi, A. Falqui, A. Musinu, G. Piccaluga, C. Sangregorio, G. Spano, Phys. Chem. Chem. Phys. 3 (2001) 832–838.
[68] K. Nadeem, H. Krenn, T. Traussnig, R. Würschum, D.V. Szabó, I. Letofsky-Papst, J. Magn. Magn. Mater. 323 (2011) 1998–2004.
[69] J. Nogués, J. Sort, V. Skumryev, S. Surinach, J.S. Munoz, M.D. Baró, Phys. Rep. 422 (2005) 65–117.
[70] X. Liang, B. Xi, S. Xiong, Y. Zhu, F. Xue, Y. Qian, Mater. Res. Bull. 44 (2009) 2233–2239.
[71] D.W. Kavich, J.H. Dickerson, S.V. Mahajan, S.A. Hasan, J.-H. Park, Phys. Rev. B 78 (2008) 174414.
[72] R. Shi, X. Liu, G. Gao, R. Yi, G. Qiu, J. Alloys Compd. 485 (2009) 548–553.
[73] B. Mao, Z. Kang, E. Wang, S. Lian, L. Gao, C. Tian, C. Wang, Mater. Res. Bull. 41 (2006) 2226–2231.
[74] K. Sharma, S. Singh, C.L. Prajapat, S. Bhattacharya, Jagannath, M.R. Singh, S.M. Yusuf, G.P. Kothiyal, J. Magn. Magn. Mater. 321 (2009) 3821–3828.
[75] M. Gotić, T. Jurkin, S. Musić, Mater. Res. Bull. 44 (2009) 2014–2021.
[76] B. Wang, Y. Song, W. Ren, W. Xu, H. Cui, J. Sol–Gel Technol. 51 (2009) 119–123.
[77] R.F.C. Marques, C. Garcia, P. Lecante, S.J.L. Ribeiro, L. Noe, N.J.O. Silva, V.S. Amaral, A. Millan, M. Verelst, J. Magn. Magn. Mater. 320 (2008) 2311–2315.
[78] T.N. Narayanan, A.P. Reena Mary, M.M. Shaijumon, Lijie Ci, P.M. Ajayan, M.R. Anantharaman, Nanotechnology 20 (2009) 055607.
[79] R. Valenzuela, M.C. Fuentes, C. Parra, J. Baeza, N. Duran, S.K. Sharma, M. Knobel, J. Freer, J. Alloys Compd. 488 (2009) 227–231.
[80] S.M. El-Sheikh, F.A. Harraz, K.S. Abdel-Halim, J. Alloys Compd. 487 (2009) 716–723.
[81] D.K. Yi, S.S. Lee, G.C. Papaefthymion, J.Y. Ying, Chem. Mater. 18 (2006) 614–619.
[82] D. Ortega, J.S. Garitaonandia, M. Ramirez-del-Solar, C. Barrera-Solano, M. Dominguez, Eur. Phys. J. D52 (2009) 19–22.
[83] M. Wu, Y. Ma, Y. Liu, H. Bi, Q. Fang, H. Niu, Q. Chen, Mater. Res. Bull. 43 (2008) 1321–1326.
[84] T.N. Shendruk, R.D. Desautels, B.W. Southern, J. Van Lierop, Nanotechnology 18 (2007) 455704.
[85] F.C. Fonseca, G.F. Goya, R.F. Jardim, N.L.V. Carreno, E. Longo, E.R. Leite, Phys. Rev. B 66 (2002) 104406.
[86] P. Gorria, M.P. Fernandez-Garcia, M. Sevilla, J.A. Blanco, A.B. Fuertes, Phys. Status Solidi RRL 3 (2009) 4–6.
[87] V. Sreeja, P.A. Joy, Mater. Res. Bull. 42 (2007) 1570–1576.
[88] J.R. Jeong, S.J. Lee, J.D. Kim, S.C. Shin, Phys. Status Solidi 241 (2004) 1593–1596.
[89] B. Aslibeiki, P. Kameli, H. Salamati, M. Eshraghi, T. Tahmasebi, J. Magn. Magn. Mater. 322 (2010) 2929–2934.
[90] F.C. Fonseca, R.F. Jardim, M.T. Escote, P.S. Gouveia, E.R. Leite, E. Longo, J. Nanopart. Res. 13 (2011) 703–710.
[91] M.B. Fernandez van Raap, F.H. Sanchez, C.E. Rodriguez Torres, L.I. Casas, A. Roig, E. Molins, J. Phys.: Condens. Matter 17 (2005) 6519–6531.
[92] D. Toulemon, B.P. Pichon, X. Cattoen, M.W.C. Man, S. Begin-Colin, Chem. Commun. 47 (2011) 11954–11956.
[93] R.D. Zysler, M. Vasquez Mansilla, D. Fiorani, Eur. Phys. J. B41 (2004) 171–175.
[94] J.A. Mydosh, Spin Glasses: An Experimental Introduction, Taylor and Francis, London, 1993, pp. 45–118.
[95] L. Neel, Ann. Geophys. 5 (1949) 99.
[96] D. Fiorani, A.M. Testa, F. Lucari, F. D'Orazio, H. Romero, Physica B 320 (2002) 122–126.